Earth and Planetary Science Letters 474 (2017) 248–256

Contents lists available at ScienceDirect

Earth and Planetary Science Letters

www.elsevier.com/locate/epsl

Westernmost Grand Canyon incision: Testing thermochronometric resolution

M. Fox [a,b,*,1], A. Tripathy-Lang [a,b], D.L. Shuster [a,b], C. Winn [c], K. Karlstrom [c], S. Kelley [d]

[a] Department of Earth and Planetary Science, University of California, Berkeley, CA, USA
[b] Berkeley Geochronology Center, 2455 Ridge Road, Berkeley, CA, USA
[c] Department of Earth and Planetary Sciences, University of New Mexico, Albuquerque, NM, USA
[d] Earth and Environmental Sciences Department, New Mexico Institute of Mining and Technology, Socorro, NM, USA

ARTICLE INFO

Article history:
Received 20 December 2016
Received in revised form 21 June 2017
Accepted 27 June 2017
Available online 18 July 2017
Editor: A. Yin

Keywords:
Grand Canyon
thermochronometry
radiation damage
LA-ICP-MS

ABSTRACT

The timing of carving of Grand Canyon has been debated for over 100 years with competing endmember hypotheses advocating for either a 70 Ma ("old") or <6 Ma ("young") Grand Canyon. Several geological constraints appear to support a "young" canyon model, but thermochronometric measures of cooling history and corresponding estimates of landscape evolution have been in debate. In particular, $^{4}He/^{3}He$ thermochronometric data record the distribution of radiogenic ^{4}He (from the ^{238}U, ^{235}U and ^{232}Th decay series) within an individual apatite crystal and thus are highly sensitive to the thermal history corresponding to landscape evolution. However, there are several complicating factors that make interpreting such data challenging in geologic scenarios involving reheating. Here, we analyze new data that provide measures of the cooling of basement rocks at the base of westernmost Grand Canyon, and use these data as a testbed for exploring the resolving power and limitations of $^{4}He/^{3}He$ data in general. We explore a range of thermal histories and find that these data are most consistent with a "young" Grand Canyon. A problem with the recovered thermal history, however, is that burial temperatures are under predicted based on sedimentological evidence. A solution to this problem is to increase the resistance of alpha recoil damage to annealing, thus modifying He diffusion kinetics, allowing for higher temperatures throughout the thermal history. This limitation in quantifying radiation damage (and hence crystal retentivity) introduces non-uniqueness to interpreting time–temperature paths in rocks that resided in the apatite helium partial retention zone for long durations. Another source of non-uniqueness, is due to unknown U and Th distributions within crystals. We show that for highly zoned with a decrease in effective U of 20 ppm over the outer 80% of the radius of the crystal, the $^{4}He/^{3}He$ data could be consistent with an "old" canyon model. To reduce this non-uniqueness, we obtain U and Th zonation information for separate crystals from the same rock sample through LA-ICP-MS analysis. The observed U and Th distributions are relatively uniform and not strongly zoned, thus supporting a "young" canyon model interpretation of the $^{4}He/^{3}He$ data. Furthermore, we show that for the mapped zonation, the difference between predicted $^{4}He/^{3}He$ data for a uniform crystal and a 3D model of the crystal are minimal, highlighting that zonation is unlikely to lead us to falsely infer an "old" Grand Canyon.

1. Introduction

The origin of Grand Canyon has been the subject of debate since the first workers attempted to understand this spectacular landform (e.g. Powell, 1879; Davis, 1901). Over the last decade, thermochronometry has emerged as a geochemical approach to measure valley incision as it does not require measuring sediment flux and identifying the source of sediments, nor does it rely on using erosional or depositional features (such as fluvial terraces) that are erased through time due to erosion (Shuster et al., 2005). Low-temperature thermochronometry is based on the temperature dependent retentivity of daughter products of radioactive decay that are sensitive to relatively low temperatures (hence near-surface depths). This approach has been extensively applied to resolve debate surrounding Grand Canyon incision. Unfortunately, the resulting conclusions have also been controversial with different datasets supporting a 70 Ma ("old") or <6 Ma ("young") Grand

* Corresponding author.
E-mail address: m.fox@ucl.ac.uk (M. Fox).
[1] Now at Department of Earth Sciences, University College London, London, UK.

http://dx.doi.org/10.1016/j.epsl.2017.06.049

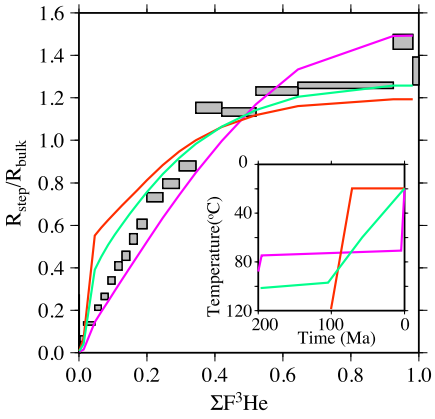

Fig. 1. $^4He/^3He$ data from the Separation Pluton in westernmost Grand Canyon. The *x*-axis is cumulative release fraction of proton-induced ^3He; *y*-axis is the R_{step}/R_{bulk} value (where R_{step} is the ratio of $^4He/^3He$ measured in a single step, R_{bulk} is the ratio of all steps summed). The data are precise due to a large abundance of Helium released in each heating step. The (U–Th)/He age of this crystal is 93.4 ± 1.43 Ma. Three reference time–temperature paths (inset) that predict this age are shown to illustrate the resolving power of the data, when assuming a spatially uniform U and Th distribution within the crystal.

Canyon (e.g., Flowers et al., 2008; Flowers and Farley, 2012, 2013; Lee et al., 2013; Karlstrom et al., 2016, 2014), as highlighted in Fig. 1. Much of this inconsistency arises because the sedimentary deposits of parts of Grand Canyon are insufficiently thick to have completely reset the applied thermochronometric systems during maximum burial conditions. Put simply, Grand Canyon incision is a difficult problem for modern methods of low-temperature thermochronometry. A companion paper by Winn et al. (2017) summarizes the debate surrounding the incision of westernmost Grand Canyon segment and highlights discrepancies amongst interpretations of thermochronometric data and geological evidence.

In the case of Grand Canyon, some of the discrepancies between different thermochronometric interpretations and geological evidence can be explained by identifying more complex landscape evolution possibilities (Karlstrom et al., 2014) or through more complex thermal histories (Fox and Shuster, 2014). Furthermore, the requirement to account for these discrepancies, combined with extensive geological constraints, makes westernmost Grand Canyon an excellent natural laboratory for exploring the limitations of the apatite (U–Th)/He thermochronometric system. In this respect, we can address the general question: what geomorphic scenarios can be excluded using high precision thermochronometric data? Here, we present a numerical analysis of apatite $^4He/^3He$ data (Winn et al., 2017) in terms of permissible time–temperature paths, and explore the possibility that much of the signal can be explained simply by changing the U and Th zonation of the crystal. We show that zonation variations can lead to dramatic differences in the time–temperature interpretation of thermochronometric data and present numerical and analytical approaches to account for this zonation.

Apatite $^4He/^3He$ thermochronometric data record the thermal history of rocks at the base of westernmost Grand Canyon with thermal resolution from ~90–30 °C (Farley, 2000; Shuster et al., 2006), and thus, for a reasonable geothermal gradient (~30 °C/km), should resolve incision of westernmost Grand Canyon. Data presented in Winn et al. (2017) and are from sample 10GC161(RM 240) are from the Paleoproterozoic Separation pluton, which crops out from RM 239.5 to 239.8 (RM = river miles downstream of Lees Ferry from Stevens, 1983). This pluton is a weakly foliated, medium grained granite that is similar to other Lower Granite Gorge plutons that range in age from 1710 to 1680 Ma (Karlstrom et al., 2003). First, we provide a brief summary of thermochronometric data from Grand Canyon, which highlight the range of geomorphic scenarios currently permitted by different thermochronometric data and interpretations. Second, we summarize the challenges faced with the interpretation of (U–Th)/He based thermochronometry in this geological setting and how this complexity provides potential to more tightly constrain thermal histories. Third, we then present the numerical methods used to maximize the amount of information we can extract from the data, but also the resolving power of the data. Finally, we present the results of our analysis and discuss the implications for the analysis of (U–Th)/He based thermochronometry in general and the Grand Canyon. Despite complicating factors and sources of uncertainty, we show that the data support a "young" Canyon model.

2. Background

2.1. Thermochronometry and Grand Canyon debate

Thermochronometry constrains the range of possible thermal histories of rocks at the base of the canyon during both burial by Paleozoic and Mesozoic strata and canyon incision, and thus can provide an *in-situ* record of landscape evolution. The transition between loss and retention of ^4He in the apatite (U–Th)/He system occurs between ~90–30 °C due changes in thermally activated diffusive loss of radiogenic ^4He (Zeitler et al., 1987; Farley, 2000; Shuster et al., 2006). Assuming a reasonable geothermal gradient (~30 °C/km), these temperatures correspond to 1–3 km. For Grand Canyon, apatite (U–Th)/He ages predicted for multiple time–temperature paths help understand the incision history (e.g., Flowers et al., 2008; Flowers and Farley, 2012; Wernicke, 2011; Lee et al., 2013; Karlstrom et al., 2014, 2016). However, these inferred time–temperature paths are non-unique, and our knowledge of the He diffusion kinetics in apatite fundamentally limits their accuracy.

Using bulk (U–Th)/He ages, Flowers et al. (2008) concluded that "the gorge and the plateau surface had similar Early to mid-Tertiary thermal histories, despite their >1500 m difference in vertical structural position... indicating that a 'proto-Grand Canyon' of kilometer-scale depth had incised post-Paleozoic strata by the Early Eocene". Wernicke (2011) hypothesized that a 70–80 Ma California River flowing NE, followed by a 55–30 Ma Arizona River flowing SW, carved Grand Canyon to within a few hundred meters of its modern depth.

Lee et al. (2013) and Karlstrom et al. (2014) presented (U–Th)/He ages and apatite fission track data (sensitive to ~110–60 °C: Carlson et al., 1999) from rim and river-level rocks in the eastern Grand Canyon that suggest different cooling histories prior to 25 Ma, but similar temperatures after 15 Ma. They interpret these data to indicate that no canyon existed in this segment until the 25–15 Ma incision of an East Kaibab paleocanyon; further, their data indicate that Marble Canyon was not incised until the last 5–6 Ma. Karlstrom et al. (2014) then proposed a paleocanyon solution in which most of modern Grand Canyon was incised by the Colorado River in the last 6 Ma. Karlstrom et al. (2016) reinforced this paleocanyon hypothesis by re-modeling thermochronometric data (from Flowers et al., 2008) from the Little Colorado River valley; these data support incision of the 25–15 Ma East Kaibab paleocanyon by a 25–15 Ma ancestral Little Colorado River. Older 70–50 Ma thermochronometric ages seen in many samples are attributed to northward cliff retreat of Mesozoic strata off the Mogollon highlands rather than carving of a 70–25 Ma Grand Canyon.

Apatite $^4He/^3He$ thermochronometry involves stepwise degassing of individual crystals that have been irradiated with energetic protons, and thus contain a spatially uniform distribution of artificial ^3He (Shuster and Farley, 2004). The results of the stepwise degassing experiment reveals the spatial distribution of ^4He within the crystal, which can then be used to constrain possible

time–temperature paths the sample might have experienced. This method was first applied to Grand Canyon by Flowers and Farley (2012), who noted a major difference between possible eastern and western Grand Canyon cooling histories. These authors concluded that 70% of westernmost Grand Canyon was carved by ~70 Ma. However, Fox and Shuster (2014) demonstrated that the ^{4}He/^{3}He data published by Flowers and Farley (2012) could also be reconciled with a "young" Canyon model, provided that burial conditions are more fully considered, as this modifies the temperature sensitivity of the crystal due to retention of alpha recoil damage (Shuster et al., 2006).

A companion paper by Winn et al. (2017) summarizes all new and published apatite thermochronometric data from westernmost Grand Canyon segment. This is the key (and formerly unresolved) segment where different thermochronometric data provide strongly conflicting results. Winn et al. summarize new (and older) geologic studies that support this segment being "young", then present new apatite ^{4}He/^{3}He data, as well as new apatite fission track and apatite (U–Th)/He ages for samples throughout this 40-mile-long corridor. This is the first time that 3 thermochronometric methods in apatite have been applied to the same rock samples in Grand Canyon. Our new ^{4}He/^{3}He data are more precise than earlier data because our sample had higher ^{4}He content. These new data are best explained by a "young" Canyon $t-T$ history with a cooling pulse at 50–70 Ma, residence at about 60 °C (~1.5 km depth) from 50–6 Ma, and cooling to surface temperatures after 6 Ma. New time–temperature models for 4 new (U–Th)/He samples, and analysis of all existing samples supports the "young" Canyon model (Winn et al., 2017).

2.2. Complications associated with the interpretation of helium-based thermochronometry

^{4}He/^{3}He thermochronometry provides information about the spatial distribution of ^{4}He within a single apatite crystal, but several factors can influence the resultant ^{4}He/^{3}He release spectrum. These factors include the time–temperature path, and the inherent spatial distributions, or zonation, of U and Th within the crystal (Farley et al., 2010), which directly governs the distribution of ^{4}He production, as well as the probabilistic emission of alpha particles from a crystal's exterior (Farley et al., 1996). In some cases, the spatial distribution of U and Th represents a primary control on the ^{4}He/^{3}He release spectrum (Fox et al., 2014), which makes inferring time–temperature information from ^{4}He/^{3}He data challenging. Thus, researchers have begun to measure the spatial distribution of U and Th within an apatite crystal using laser ablation inductively coupled plasma mass spectrometry (LA-ICP-MS) when a ^{4}He/^{3}He spectrum complex (Farley et al., 2011). By combining ^{4}He/^{3}He stepwise degassing experiments with a measure of the spatial variations in ^{4}He production rate, the accuracy of the inferred time–temperature path can increase (Flowers and Farley, 2012; Fox et al., 2014). However, in order to measure the spatial distributions of U and Th, a significant portion of the crystal must be destroyed to expose a polished section through the crystal. Therefore, the total molar abundances of U and Th, and thus the (U–Th)/He age associated with the crystal analyzed using ^{4}He/^{3}He thermochronometry is unknown. Conversely, to accurately measure the (U–Th)/He age of the same crystal, the entire crystal must be dissolved to determine the U and Th content via isotope dilution, thus eliminating any possibility of recovering the U and Th zonation patterns. In practice, it is not generally possible to measure both parent nuclide zonation and (U–Th)/He age for the same irradiated crystal as used for ^{4}He/^{3}He analysis, which introduces non-uniqueness to interpretations. From the same pluton at the same location, Flowers and Farley (2012) measured zonation in CP06-69 but inferred its age from other crystals. In this paper, we measured ^{4}He/^{3}He and the (U–Th)/He age in the same crystal, and measured U and Th zonation from different crystals from the same bedrock sample, 10GC161.

The diffusion kinetics of ^{4}He in apatite is a function of temperature, time, and the concentrations of U and Th in the crystal, easily represented as effective uranium (or [eU] = [U] + 0.24[Th], which weights the U and Th concentrations according to their relative alpha particle productivity; Gastil et al., 1967; Flowers et al., 2009). In particular, as U and Th decay to Pb, their intermediate alpha decays produce daughter-recoil radiation damage within the apatite crystal structure. As this damage accumulates at sufficiently low temperatures, the He diffusivity at a specific temperature in apatite appears to decrease over time (Shuster et al., 2006), whereas at sufficiently high temperatures, damage sites anneal, and He diffusivity has been measured to return to higher values at a specific temperature (Shuster and Farley, 2009). Further, radiation damage appears to control diffusivity in a predictable manner for inter-crystal datasets wherein each crystal has a different [eU] (e.g., Flowers et al., 2009; Green et al., 2006; Flowers, 2009; Fillon et al., 2013; Ault et al., 2009; Gautheron et al., 2013, 2009) and for intra-crystal zones of different [eU] (Fox et al., 2014). To account for this variation in ^{4}He retentivity as a function of accumulation and annealing of radiation damage, models have been developed (Shuster et al., 2006; Flowers et al., 2009; Gautheron et al., 2013). For example, the radiation damage accumulation and annealing model (RDAAM) is empirically calibrated, and assumes that the kinetics of damage annealing can be quantified in the same manner as fission track annealing in apatite (Flowers et al., 2009). However, fission damage may be fundamentally different from alpha recoil damage such that this basic assumption of RDAAM may need further scrutiny.

Because of the effects of radiation damage accumulation and annealing, a sample's prior thermal state controls ^{4}He diffusivity through time. This implies that any uncertainty in the prior thermal history will consequently produce additional uncertainty in the most recent phase of exhumation. For (U–Th)/He ages, radiation damage sensitivity to reheating produces diagnostic "(U–Th)/He age-[eU] correlations" for crystals that have experienced the same thermal history but have different [eU] values (e.g., Flowers et al., 2009; Flowers, 2009; Ault et al., 2009; Fillon et al., 2013; Gautheron et al., 2013). Therefore, a diverse range of ages may be expected for a given thermal history, especially if the thermal history is complex with sufficient time for different crystals to evolve different diffusion kinetics. In the case of ^{4}He/^{3}He thermochronometry, radiation damage can lead to complex release spectra as different *zones* within crystals might evolve to have different diffusion kinetics (Farley et al., 2011; Fox et al., 2014).

Finally, the rate of radiation damage annealing at a given temperature is not well understood. Several studies appear to indicate that annealing of alpha-recoil produced radiation damage occurs at slightly higher temperatures than that of apatite fission tracks (Green et al., 2006; Gautheron et al., 2013; Fillon et al., 2013; Fox and Shuster, 2014; Winn et al., 2017). The key parameter in the RDAAM that quantifies resistance to annealing is r_{mr0} (Ketcham et al., 2007). By changing the parameter r_{mr0} in the RDAAM, the annealing rate of radiation damage can be modified. In natural apatite, this parameter varies between 0.6 and 0.86 (Ketcham et al., 2007), and natural experiments thus far indicate values at the lower end of this range are more appropriate (Gautheron et al., 2013; Fillon et al., 2013; Fox and Shuster, 2014; Winn et al., 2017). Furthermore, there is no reason that two different apatite grains need have the same r_{mr0} possibly due to chlorine content (Gautheron et al., 2013), which poses a further source of uncertainty.

3. Methods

3.1. LA-ICP-MS mapping of parent nuclide distribution

Because we decided to dissolve the crystal analyzed for ^{4}He/^{3}He thermochronometry in order to determine the bulk (U–Th)/He age, we quantified the spatial distribution of U and Th for different apatite crystals from the same bedrock sample. We followed the LA-ICP-MS methods described in Tremblay et al. (2015), with full details provided in the data repository. Apatite crystals were orientated with the *c*-axes parallel to the mount and polished to expose a section of the apatite at approximately halfway through the *a*-axis. Laser ablation line-scans using a 20 μm diameter circular ablation spot began and ended in epoxy, thus fully traversing the crystal and the crystal boundaries. Several line scans were carried out perpendicular and parallel to the *c*-axis completely covering the exposed section. Once this exercise is completed, the result is a spatially referenced grid of ^{238}U and ^{232}Th, or [eU] measurements, which we refer to as "spots".

These measurements can then be converted to a 2D color contour map of [eU] concentration. Previously, the color contour map has been completed using an inverse-distance-weighted algorithm (e.g. Farley et al., 2011). However, this potentially smears the data and does not fully exploit redundant information obtained due to the fact that ablation spots overlap. In reality, a specific location on the polished section may be measured by multiple overlapping spots. These overlapping spots may record different average concentrations and therefore a specific location, sampled by multiple overlapping spots, could be associated with multiple spot values. In order to exploit this redundant information and thus improve resolution, we use formal inverse methods. We discretize the total space covered by an analysis into pixels of size $\Delta x \Delta y$. The concentration of the i^{th} spot in an analysis is simply the average of the values of the m pixels sampled by the spot,

$$s_i = \frac{1}{S}\sum_{j=1}^{k} p_j \Delta x \Delta y, \tag{1}$$

where s_i is the concentration within the i^{th} spot in an analysis, p_j is the concentration within a pixel located within the area defined by the spot center and radius of the spot. k is the total number of pixels that are within the i^{th} spot. Each pixel is defined using a 2D grid and therefore p_j actually indicates the coordinates of a specific pixel. A pixel is either within a spot or outside of a spot, and we do not account for the possibility that pixels are partially within a spot. This error is therefore directly related to the size $\Delta x \Delta y$ and for reasonable pixel sizes this error is expected to be small. S is the total size of the spot in this discrete form.

Since overlapping spots will sample the same pixels, expressions for each spot as a function of pixels can be combined in matrix form, along with 2D smoothness constraints:

$$\begin{pmatrix} \mathbf{A} \\ \dots \\ \lambda\nabla^2 \end{pmatrix} \mathbf{p} = \begin{pmatrix} \mathbf{s} \\ \dots \\ \mathbf{0} \end{pmatrix}, \tag{2}$$

where $\mathbf{A}$ is a matrix in which row i contains fractions of areas at columns that denote specific locations in space that are within the i^{th} spot. The summation of a row of $\mathbf{A}$ is equal to discrete area of a spot, S. $\mathbf{A}$ has ns rows, where ns is the total number of spots measured, and has np columns, where np is the number of pixels used to discretize the total area that was analyzed. The lower half of Eqn. (2) represents smoothness constraints imposed using the negative Laplacian of concentration, approximated with the finite difference method and λ accounts for the grid spacing and weighting. 0 is a vector containing zeros of length np. The smooth operator ($\lambda\nabla^2$) is $np \times np$ and each row corresponds to a single pixel. For example, if the concentration of a pixel and the four adjacent pixels are the same, the scalar product of the corresponding row and the vector $\mathbf{p}$ is equal to zero. However, as the curvature of concentration increases, this scalar product also increases. Solving Eqn. (2) minimizes the misfit, ϕ, and provides pixel concentrations that can be smooth in space and fit the data:

$$\phi = \|\mathbf{Ap} - \mathbf{s}\| + \lambda^2 \|\nabla^2 \mathbf{p} - \mathbf{0}\|. \tag{3}$$

If λ is small, the expression on the right is small and the degree of smoothness has a small effect on ϕ. The solution will fit the data well, but this solution will be sensitive to noise. In contrast, if λ is large, a smooth solution will be found, which may not fit the data well. This trade-off must be explored when choosing a value for λ and we recommend a trial and error approach. A value for λ of 0.5 was used throughout this study. Further information about this approach is provided in the Data Repository.

3.2. Numerical models of He diffusion in apatite

3.2.1. 1D spherically symmetric models

In order to explore the effects of thermal paths over geologic timescales on the (U–Th)/He system in apatite, we simulate the evolution of helium distribution within a crystal. For these calculations, we use a numerical model to solve the ^{4}He production diffusion-equation using a spherical approximation (Fechtig and Kalbitzer, 1966). The model accounts for spatially symmetric U and Th zonation within apatite on the production rate of ^{4}He, and alpha ejection, as outlined in Ketcham (2005). The evolution of diffusivity, as a function of space within the crystal and time, is calculated according to observed [eU] zonation data at specific radial positions and the RDAAM of Flowers et al. (2009). For all simulations we use parameter set 2 in RDAAM (Flowers et al., 2009), however, we also change the value of r_{mr0} in RDAAM as described below.

3.2.2. 3D models

In some cases, collapsing a 2D LA-ICP-MS map to a 1D radially symmetric concentration profile (Farley et al., 2011) leads to averaging the true concentrations and thereby reducing the range of concentration values (Fox et al., 2014). Therefore, we also use 3D numerical models to account for complex zonation patterns (Fox et al., 2014). This approach uses a multigrid method to efficiently solve the ^{4}He production and diffusion equation in three dimensions for both apatite (Fox et al., 2014) and zircon (Tripathy-Lang et al., 2015). We use this model to calculate the distribution of helium within crystals after the geological history and then to predict synthetic ^{4}He/^{3}He data that can be compared to observations. This model accounts for the presence of non-symmetric zonation within apatite crystals and the resulting radiation damage within the crystal as a function of space and time.

A 3D model can be designed from knowledge of the spatial distribution of U and Th obtained through LA-ICP-MS. Because we only measure this distribution across a single section of the crystal, values outside of this section must be extrapolated or estimated. We make an assumption that the concentration observed along the edge of the crystal in 2D is representative of the concentration across all edges of the crystal. Therefore to estimate values outside of the polished section, we linearly interpolate between the measured section value and the assumed outer boundary value. The position of the upper (i.e., above the polished section) and lower crystal (i.e., below the polished section) edges is known from grain measurements. We also assume that the shape of the upper and lower boundaries of the crystal are identical to the measured section.

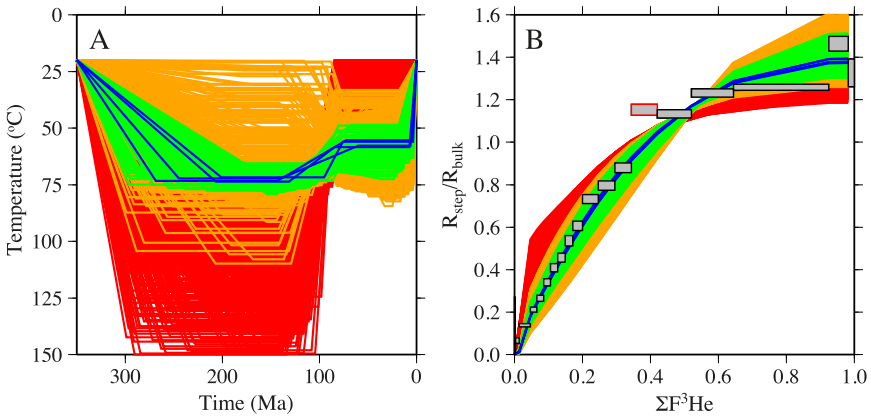

Fig. 2. Inferred time–temperature histories for Separation Pluton. (**A**) 100,000 time–temperature paths were simulated following the parameterization described in the text. 0 Ma indicates the present day. (**B**) Observed and predicted $^4He/^3He$ release spectra; axes are as defined in Fig. 1. The colored paths correspond to different misfit values between the observed and predicted data and the quality of the fit can be compared directly to the observed data. All colored time–temperature paths predict the observed (U–Th)/He age of 93.4 to within 5 Ma. Paths that were modeled but do not fit the age are not shown but these cover the entire parameter space. The heating step outlined in red in Fig. 2B was not included in the analysis and is considered an outlier here; including this datum would not significantly change the best fitting $t-T$ paths. (For interpretation of the references to color in this figure legend, the reader is referred to the web version of this article.)

4. Analysis of $^4He/^3He$ data

We explore the ability of the $^4He/^3He$ data to constrain the cooling history of bedrock now at the base of Western Grand Canyon using Monte Carlo methods. We predict synthetic ages and $^4He/^3He$ spectra for a range of time–temperature paths and 1D zonation profiles. For each model thermal history or zonation variation that fits the measured age, a synthetic $^4He/^3He$ spectrum is predicted and compared to the observed $^4He/^3He$ data. We then calculate a misfit function based on the sum of the squares of the differences between observed $^4He/^3He$ ratio and predicted $^4He/^3He$ ratio for each step weighted by the measured error for each step. These time–temperature paths, or zonation profiles, and corresponding synthetic release spectra are colored based on the misfit value (red >8; orange <8; green <5; blue <3).

4.1. Time–temperature exploration

In order to explore the temperature sensitivity of the $^4He/^3He$ data assuming no zonation, we infer a thermal history using random time–temperature paths incorporating independent knowledge of the thermal history. We use a simple time–temperature path to parameterize the thermal history and incorporate constraints, greatly reducing the number of parameters that we explore, yet maintaining the flexibility to describe both the "young" and "old" Canyon models, as outlined in Fox and Shuster (2014). In this simple parameterization, all time–temperature paths begin at 550 Ma, reflecting the Great Unconformity (Karlstrom and Timmons, 2012), and remain at surface temperatures (20 °C) until ~350 Ma reflecting the Temple Butte unconformity (Beus, 1989, 2003). The time–temperature path between 350 Ma and the present day is parameterized with six model parameters: temperature between $t1$ and $t2$ is equal to $T1$; temperature between $t3$ and $t4$ is equal to $T2$. An additional constraint is imposed at 20 °C at the present day reflecting modern surface temperatures. A specific time–temperature path is linearly interpolated between (350 Ma, 20 °C) and ($t1$, $T1$) and between ($t2$, $T1$) and ($t3$, $T2$) and also between ($t4$, $T2$) and (0 Ma, 20 °C). Temperatures are free to vary between 20 and 150 °C. And $t1$ to $t4$ are free to vary as follows: $t1$, 150–300 Ma; $t2$, 86–145 Ma; $t3$, 30–85 Ma; $t4$ 3–25 Ma. We repeat this analysis for two values of r_{mr0} in RDAAM, the canonical value of 0.83 and a lower value of 0.65, close to the lowest value reported of 0.6 (Ketcham et al., 2007).

4.2. Zonation exploration

In order to explore the influence of potentially unrecognized U and Th zonation, we hold the time–temperature path constant and allow the zonation profile to vary. Here, we test whether the data can exclude an "old" Canyon model, and therefore use an "old" Canyon time–temperature path. We define radially symmetric zonation concentration by linearly interpolating between 4 nodes. The [eU] value of a given node is free to vary and the radial positions of the two central nodes are also free to vary, the outer nodes are held at fixed locations at the center of the crystal and the edge of the crystal. For each simulation, random [eU] values are initially drawn between 0 and 1 and then the values are rescaled to the observed bulk concentration.

5. Results and discussion

5.1. $^4He/^3He$ data for 10GC161

Due to the relatively high concentration of radiogenic ^4He in crystal 10GC161c (~10^{-9} mol/g), $^4He/^3He$ ratios were measured with high precision (see Winn et al. (2017) and Table DR 2). The $^4He/^3He$ ratios for the crystal increase systematically from initially low values and produce a release spectrum (Fig. 1), which is consistent with a uniform spatial distribution of U and Th within the crystal. Because the (U–Th)/He age, along with the $^4He/^3He$ data of the same crystal provides important constraints on the thermal path, the crystal was dissolved and the (U–Th)/He age precisely determined via isotope dilution using a Neptune Plus ICP-MS, see Tremblay et al. (2015) for further details. The alpha-ejection corrected measured age of this crystal is 93.38 ± 1.43 Ma.

5.2. Time–temperature history assuming no zonation

Under the assumption of no zonation, we search for time–temperature paths that are consistent with the data, using the approach outlined in Section 4.1. We find that time–temperature paths that agree best with the new data from Separation Pluton, located at river mile 240, indicate that rocks were at relatively high temperatures, in excess of 50 °C within the last 70 Ma (Fig. 2). For this first time–temperature search we use the canonical r_{mr0} value of 0.83. These temperatures support a "young" Canyon model and suggest that Grand Canyon was incised relatively recently, although these data alone do not have resolution to identify precisely when

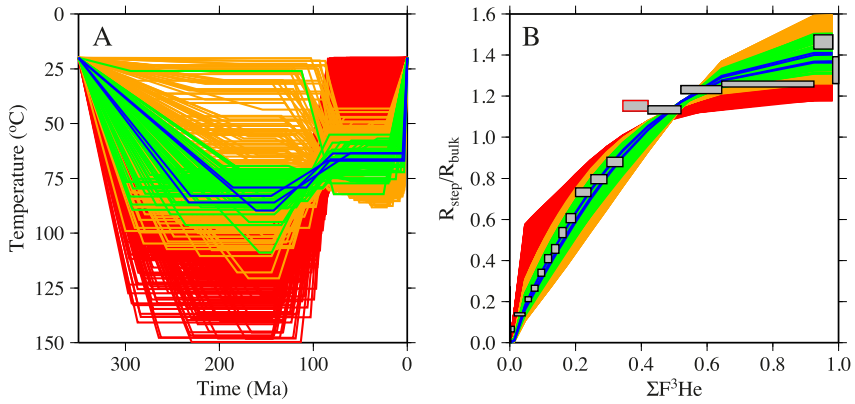

Fig. 3. Testing the effects of r_{mr0} on the inferred time–temperature history of Separation Pluton. (**A**) 100,000 time–temperature paths were simulated following the parameterization described in the text, however the r_{mr0} parameter was changed from 0.83 (Fig. 2) to 0.65, which is approximately the lower bound on observations of this parameter (Ketcham et al., 2007). (**B**) Observed and predicted $^4He/^3He$ release spectra; axes are as defined in Fig. 1. Reducing r_{mr0} has the effect of reducing the rate at which alpha recoil damage is annealed at a specific temperature, and permits higher temperatures (Fig. 3A compared to Fig. 2A) during and after burial. As in Fig. 2, the colored paths correspond to different misfit values. (For interpretation of colors in this figure legend, the reader is referred to the web version of this article.)

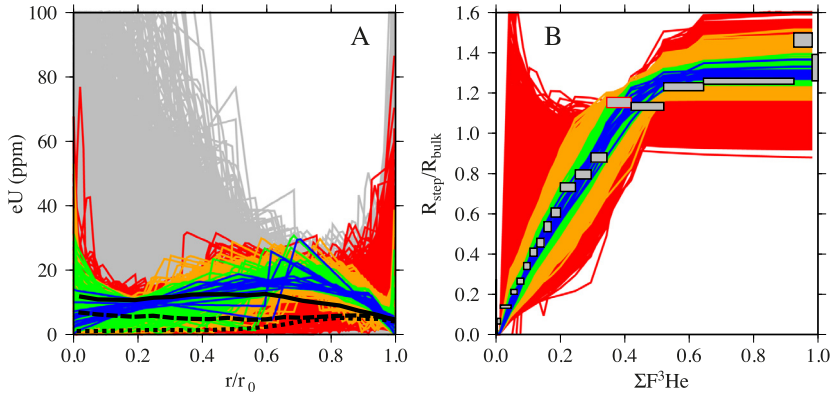

Fig. 4. Exploring the effects of U and Th zonation on sample 10GC161c from Separation Pluton. (**A**) Inferred zonation patterns that are consistent with an "old" Canyon time–temperature path (see inset of Fig. 1), the observed $^4He/^3He$ data and the bulk U and Th concentrations. [eU] = [U] + 0.24[Th] and weights the U and Th concentrations according to their relative alpha particle productivity. r/r_o is the radial position, r, normalized by the spherical equivalent radius of the crystal, $r_o = 82$ μm. The black solid, dotted and dashed curves correspond to three crystals from the same sample that are shown in the eU zonation maps measured by LA-ICP-MS (Fig. 6A–C), 7-11-GC161, 7-12-GC161 and 7-13-GC161, respectively. (**B**) Observed and predicted $^4He/^3He$ release spectra; axes are as defined in Fig. 1. The colored curves correspond to different misfit values between the observed and predicted data and the quality of the fit can be compared directly to the observed data. All colored zonation profiles predict the observed bulk [eU] and are within 5 Ma of the measured (U–Th)/He age of 10GC161c. (For interpretation of colors in this figure, the reader is referred to the web version of this article.)

that occurred. A diverse set of geologic observations indirectly support the "young" Canyon hypothesis for 5–6 Ma integration of the Colorado River from the Colorado Plateau to the Gulf of California and carving of westernmost Grand Canyon in the last 6 million years; our time–temperature paths are consistent with a 6 Ma Grand Canyon. In contrast, the observation that the data require high temperatures at 70 Ma is inconsistent with the "old" Canyon model for Western Grand Canyon. In the case of an assumed r_{mr0} value of 0.83, heating during burial was relatively minor (Fig. 2).

In the case of westernmost Grand Canyon, Fox and Shuster (2014) showed that by allowing for a range of burial temperatures and durations, a large range of recent temperatures were consistent with previously published $^4He/^3He$ data (Flowers and Farley, 2012). Therefore, the data were unable to distinguish between a "young" and "old" Canyon model. In addition, "old" Canyon time–temperature paths were correlated with time–temperature paths that required high temperatures during burial. Conversely, "young" Canyon models were correlated with low temperatures during burial. Therefore, high temperatures during burial (>100 °C; Dumitru et al., 1994; Naeser et al., 2001; Kelley et al., 2001) may suggest that the $^4He/^3He$ data are more consistent with an "old" Canyon model (Fox and Shuster, 2014). In order for $^4He/^3He$ data to be consistent with both a "young" Canyon model and higher temperatures during burial, some fraction of radiation damage that accumulated prior to burial had to be maintained during burial. This can be achieved by decreasing the rate at which radiation damage is annealed with a lower value of r_{mr0} (Fox and Shuster, 2014).

Therefore, we carried out another search of time–temperature space, changing the value of r_{mr0} from 0.83 to 0.65 (Fig. 3). The resulting time–temperature paths are similar to the results obtained for a r_{mr0} value of 0.83, however temperatures during burial are higher. Importantly, these burial conditions are more consistent with the apatite fission track data from the same location (see Winn et al., 2017). Furthermore, the small number of short fission tracks in 10GC86 (river mile 243, see Winn et al., 2017) indicates that burial conditions were insufficient to completely anneal all fission tracks in that sample. This suggests that temperatures during burial were somewhere in between the two temperatures that we infer for the two extreme values of r_{mr0} and hence about 80–90 °C.

5.3. Considering the effects of U and Th zonation

We next search for zonation profiles that would predict an "old" Canyon model using the approach outlined in section 4.2. We find

that an "old" Canyon model is only compatible with the data under extreme, and specific, zonation conditions (Fig. 4), with [eU] increasing from <5 ppm to ~20 ppm within the outermost 20% of the crystal. Ideally we would know the (U–Th)/He age, the ^{4}He/He spectrum, and the U and Th distribution within the same crystal; however, as discussed above, information on all three is currently not possible using modern analytical tools. Therefore, we must estimate U and Th zonation from separate apatite crystals from the same bedrock sample.

The concentration of induced fission tracks is proportional to the concentration of [eU] (Ketcham, 2005). AFT mounts of 10GC161 show limited zonation of fission tracks; qualitative assessment of this zonation indicates no more than 2–3 fold changes in U concentration for any apatite in the AFT mount (Fig. 5). This suggests that the zonation is not as extreme as required for the ^{4}He/^{3}He data to be consistent with an "old" Canyon model. Furthermore, LA-ICP-MS data from crystals from CP06-69 (RM 240), which is from the same granite and was collected by Flowers and Farley (2012) in a same location, also show no clear indications of the degree of radially symmetric zonation required for the data to be consistent with an "old" Canyon time–temperature path. We note, however, that other, more complex 3D zonation functions may enable the data to be consistent with an "old" Canyon time–temperature path and we explore this possibility below.

5.3.1. 3D zonation models

We measured the distribution of [eU] in three apatite crystals from 10GC161 using LA-ICP-MS, reported in the Data Repository. We test whether this degree of zonation would have an appreciable effect on the ^{4}He/^{3}He spectrum by designing 3D numerical models of these three crystals. These 3D models allow us to further explore the importance of zonation because zones can be poorly approximated with 1D radially symmetric models, which often dampen out [eU] differences across a crystal due to spatial averaging (Fox et al., 2014). For each 3D model, we predict two ^{4}He/^{3}He release spectra for an "old" Canyon model: one with spatially variable zonation and one with no zonation, setting the entire crystal to the same average [eU] value, Fig. 6.

7-11-GC161: The first crystal is relatively small and has a size of 152.8 × 87.8 × 87.8 μm, however the third dimension is estimated. 194 laser spot measurements were collected at the Berkeley Geochronology Center with spot size of 20 μm diameter and the center of these spots are shown in Fig. 6A. The area covered by the crystal was divided into 65 × 65 pixels of size 3.03 μm and eU concentrations were determined for each pixel using Eqn. (2) to produce a continuous map. The map is relatively "blotchy" and no clear zones are identified. A value of 5 ppm was prescribed as the upper and lower crystal boundary, and we acknowledge that this represents a major source of uncertainty in our models. Simulating the 3D production–diffusion of He for an "old" canyon time–temperature path predicts the synthetic ^{4}He/^{3}He spectrum shown in Fig. 6D. This predicted release spectrum is very similar to a uniform model (Fig. 6D). This suggests that if crystal 10GC161c (chosen for ^{4}He/^{3}He analysis) had similar zonation to 7-12-GC161, the influence of [eU] zonation is minimal, and the "old" Canyon model would not predict a spectrum in agreement with the observed data.

7-12-GC161: The second crystal is slightly larger and is 289 × 109 × 109 μm. In this case, 415 laser spot measurements were obtained (Fig. 6B). The area covered by the crystal was divided into 65 × 65 pixels of size of 4.85 μm. The map shows a clear zone of relatively high [eU] around the edge of the crystal with values as high as 20 ppm in this zone and low values of 1 ppm within this outer zone. A value of 20 ppm was chosen as the upper and lower crystal boundary. In this instance, the predicted release spectra for the spatially variable and the uniform 3D crystal are quite different (Fig. 6E). This suggests that if the crystal chosen for ^{4}He/^{3}He analysis has zonation similar to 7-12-GC161, we may have inferred the incorrect history. However, despite this sensitivity, even when assuming this zonation pattern, the "old" Canyon model would not predict the observed ^{4}He/^{3}He data.

7-13-GC161: The third crystal is also relatively small and has a size of 184.3 × 96.5 × 96.5 μm and concentrations were measured with 201 laser spot measurements, Fig. 6C. The area covered by the crystal was divided into 65 × 65 pixels which gives pixel sizes of 3.03 μm. A value of 10 ppm was chosen as the upper and lower crystal boundary. The resulting release spectrum for an "old" Canyon time–temperature path for both a spatially variable and uniform crystal are very similar (Fig. 6F).

An important observation is when each of these zonation patterns is assumed, the "old" Canyon model in all cases fails to predict the very low ^{4}He/^{3}He ratios observed at the beginning of the analysis (Fig. 6). To further explore potential influence of eU zonation, we also convert the observed 2D eU distributions (Fig. 6) into 1D radially symmetric zonation profiles using the approach of Farley et al. (2011). These profiles are shown in Fig. 4A as the black curves. These curves do not follow the general trend of the zonation profiles that are required for the data to be consistent with an "old" Canyon model. This further supports our assumption that the influence of zonation is unlikely to influence our interpretation in this instance.

Collecting radially symmetric concentration profiles using LA-ICP-MS can lead to a smearing of zonation data. U and Th zonation controls the spatial production of ^{4}He, which is then modified by long stopping distances of alpha particles (~20 μm; Farley et al., 1996) and temperature dependent diffusion (Shuster and Farley, 2004). In turn, if the eU zonation data are artificially dampened due to numerical interpretation methods, we could overestimate the degree of diffusion of ^{4}He and incorrectly infer an "old" canyon model. We have attempted to account for two sources of smearing of zonation information. First, large LA-ICP-MS spot sizes (20 μm in diameter) lead to averaging of information and the loss of resolution. By accounting for large spot sizes using formal inverse methods designed to deconvolve smearing, we have recovered sharper gradients in zonation. Second, collapsing 2D maps into 1D radially symmetric zonation profiles decreases the observed range in [eU] but also the rate of change of variations in [eU] (Fox et al., 2014). To account for this we have also built 3D models from the 2D maps. This reduces the degree of averaging, however does require extrapolating data from 2D to 3D. Importantly these 3D models highlight that for two of the three crystals analyzed, the range of measured [eU] values and the spatial distribution of eU concentration, the effects of zonation are unlikely to be a significant source of uncertainty.

6. Conclusions

Western Grand Canyon provides important tests of thermochronometric resolution for complex time–temperature paths. The debate on how to reconcile geologic observations and thermochronology makes this an especially important and informative field laboratory. We conclude the following:

1) U and Th zonation in apatite introduces a source of uncertainty for ^{4}He/^{3}He thermochronometry that, in general, is challenging to accommodate, as highlighted in Fig. 4. We can only measure two of the three quantities that would be most desirable (a precise (U–Th)/He age, the distribution of ^{4}He through ^{4}He/^{3}He analysis, and the U and Th spatial distribution). Therefore, crystals from the same sample are required using present methodologies to obtain an estimate of the third measurement. One potential future solution may be to obtain precise spatial distributions of

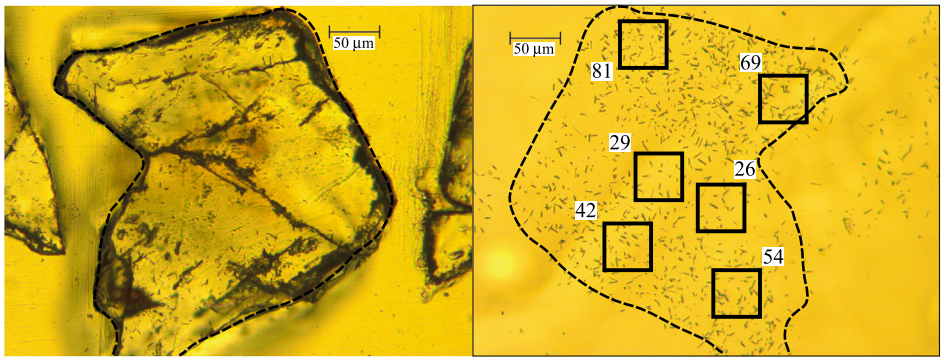

Fig. 5. Example of a fission track mount from Separation Pluton showing relatively uniform distributions of induced tracks. The left photograph shows the apatite crystal in the fission track mount and the right photograph shows induced tracks in muscovite. The outline of the crystal is shown as the dashed line. Muscovite is placed on top of the polished fission track mount prior to neutron irradiation. Therefore, the muscovite contains information about the relative concentration of ^{235}U (produced during irradiation) and the image is mirrored. Numbers show the number of induced fission tracks within 50 µm × 50 µm boxes. These relatively uniform distributions indicate that there are no extreme variations in U zonation.

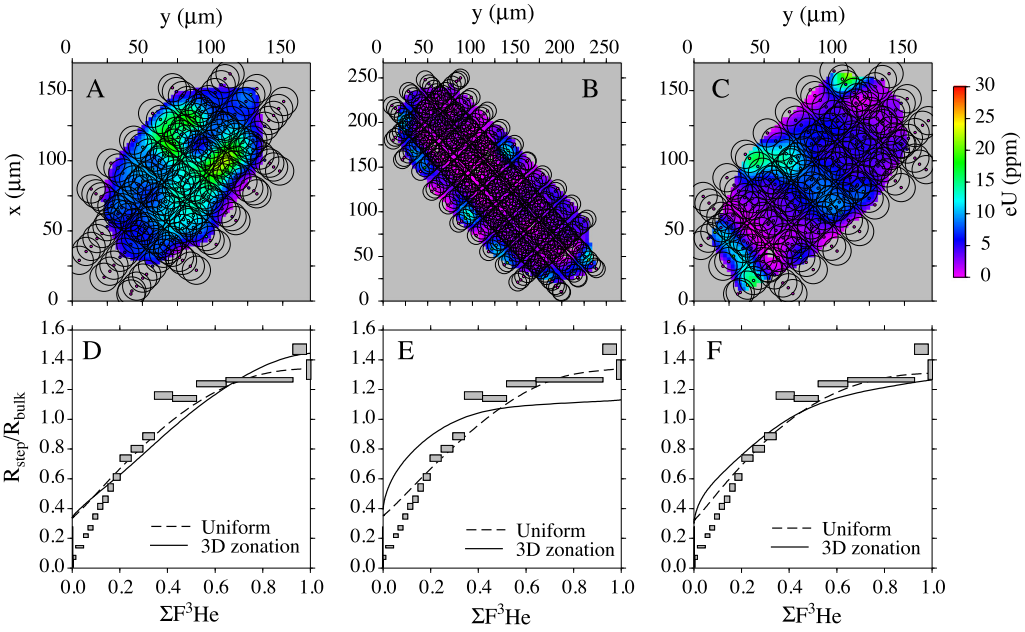

Fig. 6. U and Th zonation data from Separation Pluton along with 3D helium production diffusion model predictions of ^{4}He/^{3}He release spectra. (**A–C**) LA-ICP-MS data from crystals 7-11-GC161 (A), 7-12-GC161 (B) and 7-13-GC161 (C). The measured values are shown as [eU] plotted at the center of the ablation spots (shown as open circles, which represent the total area ablated for a single spot measurement). Overlapping circles highlight redundant information. The underlying 2D color maps correspond to the measured concentrations, as obtained from a linear inversion of the data designed to account for smearing due to the large size of the spots, Eqn. (2). Note the differing horizontal scale of each panel. (**D–F**) ^{4}He/^{3}He release spectra for the respective 3D crystal models solving the ^{4}He production–diffusion equation. Two release spectra are calculated for each crystal utilizing an "old" Canyon time–temperature path: one with spatially variable [eU] and diffusion kinetics; the second with uniform [eU] set to the bulk value. Also shown for comparison in each panel are the observed ^{4}He/^{3}He data for 10GC161c. Axes are as defined in Fig. 1.

the (U–Th)/He "ages" within a single crystal using in situ methods (Tripathy-Lang et al., 2013; Vermeesch et al., 2012).

2) New data from westernmost Grand Canyon support a "young" Canyon model where rocks cooled from 80 to 50 °C in the Laramide, resided at about 50 °C, then cooled to near surface temperatures in the last 6 Ma (Fig. 3A). Analysis of the same ^{4}He/^{3}He data using HeFTy (Ketcham, 2005) is presented by Winn et al. (2017) and the results are very similar despite differences in time–temperature path parametrization. However, if the U and Th zonation in our analyzed crystal was both specific and extreme, an "old" Canyon model could predict the observations. We conclude that this is unlikely because we found fairly uniform concentrations and modest zonation variations in crystals from the same bedrock sample. Similar results showing limited zonation were found from AFT qualitative analysis and by Flowers and Farley (2012) from several crystals from a nearby bedrock sample. Therefore, we conclude that the combined datasets are best explained by thermal paths associated with "young" Canyon incision.

3) Changing the modeled resistance to annealing of radiation damage, via r_{mr0}, leads to variations in the inferred time–temperature paths that can vary by at least 20 °C. Changing r_{mr0} from 0.83 to 0.65 increases post-Laramide residence temperatures of our samples by about 20 °C. This parameter is relatively poorly calibrated for the annealing of alpha recoil damage in apatite and may vary from crystal to crystal. However, despite this uncertainty, the new ^{4}He/^{3}He data are most consistent with a "young" Canyon model.

Acknowledgements

Research was funded in part by NSF grants EAR-1347990 (to DLS) and EAR-1348007 (to KK) from the Tectonics Program, the Ann and Gordon Getty Foundation (to DLS), the NERC

grant (NE/N015479/1 to MF) Swiss National Science Foundation (P2EZP2_148793 to MF). We thank A. Yin and two anonymous reviewers for helpful suggestions. We thank N. Fylstra for assistance with lab work at the Berkeley Geochronology Center. We also thank W. Sharp and K. Cuffey for stimulating discussions regarding LA-ICP-MS data and deconvolving laser spots.

Appendix A. Supplementary material

Supplementary material related to this article can be found online at http://dx.doi.org/10.1016/j.epsl.2017.06.049.

References

Ault, A.K., Flowers, R.M., Bowring, S.A., 2009. Phanerozoic burial and unroofing history of the Western Slave Craton and Wopmay orogen from apatite (U–Th)/He thermochronometry. Earth Planet. Sci. Lett. 284 (1), 1–11.

Beus, S.S., 1989. Devonian and Mississippian geology of Arizona. In: Geologic Evolution of Arizona. In: Arizona Geological Society Digest, vol. 17, pp. 287–311.

Beus, S.S., 2003. Temple Butte Formation. In: Beus, S.S., Morales, M. (Eds.), Grand Canyon Geology, second edition. Oxford University Press, pp. 107, 114.

Carlson, W.D., Donelick, R.A., Ketcham, R.A., 1999. Variability of apatite fission-track annealing kinetics, I: experimental results. Am. Mineral. 84, 1213–1223. http://dx.doi.org/10.2138/am-1999-0901.

Davis, W.M., 1901. An excursion to the Grand Canyon of the Colorado. Harv. Coll. Mus. Zool. Bull. 38, 107–201.

Dumitru, T.A., Duddy, I.R., Green, P.F., 1994. Mesozoic–Cenozoic burial, uplift, and erosion history of the west-central Colorado Plateau. Geology 22 (6), 499–502.

Farley, K.A., 2000. Helium diffusion from apatite: general behavior as illustrated by Durango fluorapatite. J. Geophys. Res. 105 (B2), 2903–2914.

Farley, K.A., Wolf, R.A., Silver, L.T., 1996. The effects of long alpha-stopping distances on (U–Th)/He ages. Geochim. Cosmochim. Acta 60, 4223–4229.

Farley, K.A., Shuster, D.L., Watson, E., Wanser, K., Balco, G., 2010. Numerical investigations of apatite ^{4}He/^{3}He thermochronometry. Geochem. Geophys. Geosyst. 11 (10).

Farley, K.A., Shuster, D.L., Ketcham, R.A., 2011. U and Th zonation in apatite observed by laser ablation ICPMS, and implications for the (U–Th)/He system. Geochim. Cosmochim. Acta 75 (16), 4515–4530.

Fechtig, H., Kalbitzer, S., 1966. The diffusion of argon in potassium-bearing solids. In: Schaeffer, A., Zaehhinger, J. (Eds.), Potassium Argon Dating. Springer, pp. 68–107.

Fillon, C., Gautheron, C., van der Beek, P., 2013. Oligocene–Miocene burial and exhumation of the Southern Pyrenean foreland quantified by low-temperature thermochronology. J. Geol. Soc. 170 (1), 67–77.

Flowers, R.M., 2009. Exploiting radiation damage control on apatite (U–Th)/He dates in cratonic regions. Earth Planet. Sci. Lett. 277 (1), 148–155.

Flowers, R.M., Farley, K.A., 2012. Apatite ^{4}He/^{3}He and (U–Th)/He evidence for an ancient Grand Canyon. Science 338, 1616–1619.

Flowers, R.M., Farley, K.A., 2013. Response to Comments on "Apatite ^{4}He/^{3}He and (U–Th)/He evidence for an Ancient Grand Canyon". Science 340, 143. http://dx.doi.org/10.1126/science.1234203.

Flowers, R.M., Wernicke, B.P., Farley, K.A., 2008. Unroofing, incision, and uplift history of the southwestern Colorado Plateau from apatite (U–Th)/He thermochronometry. Geol. Soc. Am. Bull. 120, 571–587.

Flowers, R.M., Ketcham, R.A., Shuster, D.L., Farley, K.A., 2009. Apatite (U–Th)/He thermochronometry using a radiation damage accumulation and annealing model. Geochim. Cosmochim. Acta 73, 2347–2365.

Fox, M., Shuster, D.L., 2014. The influence of burial heating on the (U–Th)/He system in apatite: Grand Canyon case study. Earth Planet. Sci. Lett. 397, 174–183.

Fox, M., McKeon, R.E., Shuster, D.L., 2014. Incorporating 3-D parent nuclide zonation for apatite ^{4}He/^{3}He thermochronometry: an example from the Appalachian Mountains. Geochem. Geophys. Geosyst. 15 (11), 4217–4229.

Gastil, R.G., Delisle, M., Morgan, J., 1967. Some Effects of Progressive Metamorphism on Zircons. Geol. Soc. Am. Bull. 78, 879.

Gautheron, C., Tassan-Got, L., Barbarand, J., Pagel, M., 2009. Effect of alpha-damage annealing on apatite (U–Th)/He thermochronology. Chemical Geology 266 (3), 157–170.

Gautheron, C., Barbarand, J., Ketcham, R.A., Tassan-Got, L., van der Beek, P., Pagel, M., Pinna-Jamme, R., Couffignal, F., Fialin, M., 2013. Chemical influence on α-recoil damage annealing in apatite: implications for (U–Th)/He dating. Chem. Geol. 351, 257–267.

Green, P.F., Crowhurst, P.V., Duddy, I.R., Japsen, P., Holford, S.P., 2006. Conflicting (U–Th)/He and fission track ages in apatite: enhanced He retention, not anomalous annealing behaviour. Earth Planet. Sci. Letters 250 (3), 407–427.

Karlstrom, K.E., Timmons, J.M., 2012. Many Unconformities Make One Great Unconformity. Geological Society of America Special Papers, vol. 489, pp. 73–79.

Karlstrom, K.E., Ilg, B.R., Williams, M.L., Hawkins, D.P., Bowring, S.A., Seaman, S.J., 2003. Paleoproterozoic rocks of the Granite Gorges. In: Beus, S.S., Morales, M. (Eds.), Grand Canyon Geology, second edition. Oxford University Press, pp. 9–38.

Karlstrom, K.E., Lee, J.P., Kelley, S.A., Crow, R.S., Crossey, L.J., Young, R.A., Lazear, G., Beard, S.L., Ricketts, J.W., Fox, M., Shuster, D.L., 2014. Formation of the Grand Canyon 5 to 6 million years ago through integration of older palaeocanyons. Nat. Geosci. 7, 239–244.

Karlstrom, K.E., Crossey, L.J., Embid, E., Crow, R., Heizler, M., Hereford, R., Beard, L.S., Ricketts, J.W., Cather, S., Kelley, S., 2016. Cenozoic incision history of the Little Colorado River: its role in carving Grand Canyon and onset of rapid incision in the last ~2 Ma in the Colorado River System: Geosphere CRevolution volume. Geosphere 13 (1), 1–33.

Kelley, S.A., Chapin, C.E., Karlstrom, K.E., 2001. Laramide cooling histories of Grand Canyon, Arizona, and the Front Range, Colorado, determined from apatite fission-track thermochronology. In: Colorado River: Origin and Evolution. Grand Canyon, Arizona, Grand Canyon Association, pp. 37–42.

Ketcham, R.A., 2005. Forward and inverse modeling of low-temperature thermochronometry data. Rev. Mineral. Geochem. 58 (1), 275–314.

Ketcham, R.A., Carter, A., Donelick, R.A., Barbarand, J., Hurford, A.J., 2007. Improved modeling of fission-track annealing in apatite. Am. Mineral. 92 (5–6), 799–810.

Lee, J.P., Stockli, D.F., Kelley, S.A., Pederson, J.L., Karlstrom, K.E., Ehlers, T.A., 2013. New thermochronometric constraints on the Tertiary landscape evolution of the central and eastern Grand Canyon, Arizona. Geosphere 9, 216–228. http://dx.doi.org/10.1130/GES00842.1.

Naeser, C., Duddy, I., Elston, D., Dumitru, T., Green, P., 2001. Fission-track analysis of apatite and zircon from Grand Canyon, Arizona, Colorado River origin and evolution: Grand Canyon National Park, Grand Canyon, Arizona. Grand Canyon Association, pp. 31–36.

Powell, J.W., 1879. Report on the Arid Regions of the United States with a More Detailed Account of the Lands of Utah. U.S. Geographical and Geological Survey of the Rocky Mountain region, U.S. Government Printing Office. 195 p.

Shuster, D.L., Farley, K.A., 2004. ^{4}He/^{3}He thermochronometry. Earth Planet. Sci. Lett. 217, 1–2.

Shuster, D.L., Ehlers, T.A., Rusmore, M.E., Farley, K.A., 2005. Rapid glacial erosion at 1.8 Ma revealed by ^{4}He/^{3}He thermochronometry. Science 310, 1668–1670.

Shuster, D.L., Flowers, R.M., Farley, K.A., 2006. The influence of natural radiation damage on helium diffusion kinetics in apatite. Earth Planet. Sci. Lett. 249 (3), 148–161.

Shuster, D.L., Farley, K.A., 2009. The influence of artificial radiation damage and thermal annealing on helium diffusion kinetics in apatite. Geochim. Cosmochim. Acta 73 (1), 183–196.

Stevens, L.E., 1983. The Colorado River in Grand Canyon: A Comprehensive Guide to its Natural and Human History. Red Lake Books, Flagstaff, Ariz, 107 p.

Tremblay, M.M., Fox, M., Schmidt, J.L., Tripathy-Lang, A., Wielicki, M.M., Harrison, T.M., Zeitler, P.K., Shuster, D.L., 2015. Erosion in southern Tibet shut down at ~10 Ma due to enhanced rock uplift within the Himalaya. Proc. Natl. Acad. Sci. USA 112 (39), 12030–12035.

Tripathy-Lang, A., Fox, M., Shuster, D.L., 2015. Zircon ^{4}He/^{3}He thermochronometry. Geochim. Cosmochim. Acta 166, 1–14.

Tripathy-Lang, A., Hodges, K.V., Monteleone, B.D., Soest, M.C., 2013. Laser (U–Th)/He thermochronology of detrital zircons as a tool for studying surface processes in modern catchments. J. Geophys. Res., Earth Surf. 118 (3), 1333–1341.

Vermeesch, P., Sherlock, S.C., Roberts, N.M., Carter, A., 2012. A simple method for in-situ U–Th–He dating. Geochim. Cosmochim. Acta 79, 140–147.

Wernicke, B.P., 2011. The California River and its role in carving Grand Canyon. GSA Bull. 123, 1288–1316.

Winn, C., Karlstrom, K.E., Shuster, D.L., Kelley, S., Fox, M., 2017. 6 Ma age of carving Westernmost Grand Canyon: Reconciling geologic data with combined AFT, (U–Th)/He, and ^{4}He/^{3}He thermochronologic data. Earth Planet. Sci. Lett. 474, 257–271. This issue. http://dx.doi.org/10.1016/j.epsl.2017.06.051.

Zeitler, P., Herczeg, A., McDougall, I., Honda, M., 1987. U–Th–He dating of apatite: a potential thermochronometer. Geochim. Cosmochim. Acta 51 (10), 2865–2868.